Influence of polymer molar mass and mixture stoichiometry on polyelectrolyte complexes of poly(l-arginine) and Poly(l-glutamic acid)

Polymer 263 (2022) 125497

Contents lists available at ScienceDirect

Polymer

journal homepage: www.elsevier.com/locate/polymer

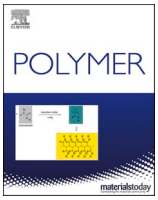

Influence of polymer molar mass and mixture stoichiometry on polyelectrolyte complexes of poly(L-arginine) and Poly(L-glutamic acid)

Valeria Castelletto [a,*], Lucas de Mello [a], Foteini Arfara [b], Hermis Iatrou [b], Jani Seitsonen [c], Ian W. Hamley [a]

[a] School of Chemistry, Pharmacy and Food Biosciences, University of Reading, Whiteknights, Reading, Berkshire, RG6 6AD, UK
[b] University of Athens, Department of Chemistry, Panepistimiopolis Zografou, 157 71, Athens, Greece
[c] Nanomicroscopy Center, Aalto University, Puumiehenkuja 2, FIN-02150, Espoo, Finland

A B S T R A C T

Poly(L-arginine) (PARG) and poly(L-glutamic acid) (PLGA) homopolypeptides were custom synthesized by precision *N*-carboxyanhydride ring-opening polymerization methods with two molar masses, matched for pairs of cationic and anionic polypeptides (degrees of polymerization $n = 100$ and $n = 500$). The conformations of the homopolypeptides were probed using circular dichroism (CD) and FTIR spectroscopy which revealed the presence of mainly polyproline II (PPII) conformation. Small-angle X-ray scattering (SAXS) showed concentration-dependent polyelectrolyte peaks and form factor with high q scaling due to the excluded volume behaviour of the wormlike chains. We then examined polyelectrolyte complexation in mixtures of pairs of PARG and PLGA polypeptides with matched molar masses. Precipitation was generally observed and the structures of precipitates, supernatant and resuspended precipitates were investigated using CD, SAXS and cryo-TEM. These revealed that, contrary to prior suggestions in the literature, the precipitates contain mostly polypeptides in a PPII-like conformation, and there is only a minimal β-sheet content (which is enhanced upon drying the sample during preparation for certain measurements). The precipitates have a fractal-like structure as revealed by cryo-TEM and SAXS. Our findings on the structure of polypeptide complex precipitates contribute to the understanding of phase separation of polyelectrolyte complexes and coacervation and may shed light on the formation of inter-cellular bodies of proteins and peptides such as Lewy and other inclusion bodies.

1. Introduction

Natural biomolecules including nucleic acids and proteins are by nature polyelectrolytes and oppositely charged biopolymers of this type can associate in solution. Polyelectrolyte complexes can form *in vivo* (in membraneless organelles), and have been proposed to have a possible role as 'protocells' in the pre-cellular evolution of living systems [1–7]. They have attracted considerable recent interest in these respects, and also in the development of membrane-free compartmentalized structures for encapsulation and other applications [4,7–10]. Polyelectrolyte complexation can lead to the formation of coacervates (liquid complexes) or solid precipitates via phase separation processes [11–14]. Precipitates are kinetically trapped structures that result from ion pair interactions between 'stronger' polyelectrolytes [14]. The formation of liquid as opposed to solid complexes depends on a number of factors including the strength of the polyelectrolyte and the chirality of the polymer. Tirrell and coworkers reported in a study on poly(lysine) and poly(glutamic acid) that liquid coacervates are formed with random racemic D, L-polymers whereas complexes of homochiral versions (L- or D-enantiomers) of these polymers formed solid precipitates, this being ascribed to the ability of the oppositely charged polypeptides to form aggregating β-sheets [15,16]. Complexation of polyelectrolytes is favourable, due to enthalpic electrostatic interactions but predominantly arising from the entropy increase associated with counterion release [14,17,18].

Synthetic polymers including homopolypeptides and others offer advantages in the study of the physical chemistry of polyelectrolyte complexation in that the sequence and charge distribution are specified by design, for example they are fully repetitive for homopolyelectrolytes. In previous work, many examples of synthetic polyelectrolytes have been used. Model polyanionic polymers include poly(glutamic acid), (especially poly(L-glutamic acid), PLGA), poly(acrylic acid) (both usually available as sodium salts) or poly(styrene sulfonate) while model cationic polyelectrolytes studied include poly(L-lysine), poly(allylamine hydrochloride) or poly(diallyldimethylammonium) (prepared as halide salts) [7,9,14,19–23]. Here, we study polyelectrolyte complexation of poly(L-glutamic acid) and poly(L-arginine) (PARG) (structures shown in SI Scheme S1). PARG has been relatively less widely investigated as a model polyelectrolyte. Due to the presence of highly basic guanidinium groups, it is expected to behave as a strong polyelectrolyte [14]. In

* Corresponding author.
E-mail address: v.castelletto@reading.ac.uk (V. Castelletto).

https://doi.org/10.1016/j.polymer.2022.125497
Received 13 September 2022; Received in revised form 25 October 2022; Accepted 3 November 2022
Available online 14 November 2022

Table 1
Molecular characteristics of the synthesized deprotected homopolypeptides.

Polymer	M_n x 10^{-3} [a]	$M_{n,stoich}$ x 10^{-3}	Đ
$PARG_{100}$	16.1	15.6	1.11
$PARG_{500}$	75.5	78.0	1.21
$PLGA_{100}$	13.1	12.9	1.09
$PLGA_{500}$	62.1	64.5	1.23

[a] Obtained by SEC-TALLS using as a carrier solvent a mixture of 0.10% TFA (v/v) solution of water/acetonitrile (80/20 v/v) at a flow rate of 0.8 mL min^{-1} at 35 °C.

contrast, PLGA as a poly(carboxylic acid) is classed as a weak polyelectrolyte [14]. PARG is of interest both as a model cationic polyelectrolyte and also due to potential applications in cell-penetrating peptides for delivery of nucleic acids and in antimicrobial materials.

Here we show that PARG and PLGA (both with two molar masses, custom synthesized) form solid precipitate complexes. The structure of the complexes is investigated as a function of the mixture stoichiometry (net charge) using cryogenic-transmission electron microscopy (cryo-TEM) and small-angle X-ray scattering (SAXS), and changes in the polypeptide conformations upon complexation are examined using FTIR and circular dichroism spectroscopy, as well as X-ray diffraction.

2. Experimental

2.1. Synthesis

Polyelectrolytes poly(L-glutamic acid) (PLGA) and poly(L-arginine) (PARG) were synthesized using *N*-carboxyanhydride (NCA) ring-opening polymerization chemistry, as detailed in the SI. For each polymer, two molar masses corresponding to degrees of polymerization n = 100 and n = 500 were prepared. The molar masses and dispersity indices are provided in Table 1. These molar masses were selected as being suitable for possible applications, and also for comparison with work from Tirrell's group who studied PLGA and P(L-lysine) (and other enantiomers) with n = 100 and n = 400 [7,16].

The deprotected polypeptides were characterized by NMR spectroscopy and Size Exclusion Chromatography (SEC).

2.2. NMR spectroscopy

^{1}H NMR measurements were performed with a 400 MHz Bruker Avance Neo instrument. Deuterium oxide (D_2O) was used as the solvent for the deprotected polypeptides, while deuterated chloroform ($CDCl_3$) was employed as the solvent for NCAs as well as the protected polypeptides, at room temperature. NMR spectra are shown in SI Fig. S1 and SI Fig. S2 for PLGA and PARG respectively. The results reveal that the poly(L-arginine) is 96% deprotected, while the poly(L-glutamic acid) is 99% deprotected.

2.3. Size Exclusion Chromatography

Size exclusion chromatography (SEC) was employed to determine the weight-average molar mass M_w and dispersity $Đ = M_w/M_n$ values. The analysis was performed using a Waters Breeze instrument equipped with a 2410 differential refractometer and a Precision PD 2020 two angle (15°, 90°) light scattering detector. The carrier solvent was a 0.10% TFA (v/v) solution of water/acetonitrile (80/20 v/v) at a flow rate of 0.8 mL min^{-1} at 35 °C. Three linear Waters hydrogel columns were used as a stationary phase. The SEC elugrams of the deprotected homopolypeptides are shown in SI Fig. S3.

2.4. Sample preparation

Solutions of pure $PARG_{100}$, $PARG_{500}$, $PLGA_{100}$ and $PLGA_{500}$ were prepared by adding weighed amounts of material into weighed amounts of water, followed by 15 min of sonication in an ultrasound water bath. Binary solutions, containing $PARG_x$/$PLGA_x$ (x = 100 or 500) at net charge 0 or -0.5 (calculated using the Henderson-Hasselbalch equation [24]), were prepared by mixing controlled volumes of pure $PARG_x$ or $PLGA_x$ solutions. Binary solutions were vortexed for 15 s, immediately after their component solutions were mixed. Mixing equal amounts of 2.2 wt% $PARG_x$ and 2.6 wt% $PLGA_x$ solutions, provided a 1.1 wt% $PARG_x$:1.3 wt% $PLGA_x$ mixture with net charge 0. Similarly, mixing equal amounts of 1 wt% $PARG_x$ and 0.6 wt% $PLGA_x$ solutions, provided a 0.5 wt% $PARG_x$:0.3 wt% $PLGA_x$ solution with net charge = −0.5.

2.5. Circular dichroism (CD) spectroscopy

CD spectra were recorded using a Chirascan spectropolarimeter (Applied Photophysics, Leatherhead, UK). Solutions were placed between parallel plates (0.01 mm path length). Spectra were measured with 0.5 nm step, 0.5 nm bandwidth, and 1 s collection time per step. The CD signal from the water background was subtracted from the CD data of the sample solutions. CD signals were smoothed using the Chirascan software for data analysis. The residue of the calculation was chosen to oscillate around the average, to avoid artifacts in the smoothed curve.

2.6. Fourier transform infrared (FTIR) spectroscopy

Spectra were recorded using a Thermo-Scientific Nicolet iS5 instrument equipped with a DTGS detector, with a Specac Pearl liquid cell (samples in D_2O contained between fixed CaF_2 plates). Spectra were scanned 116 times over the range 900–4000 cm^{-1}.

2.7. Polarized optical microscopy (POM)

Experiments were performed using an Olympus BX41 polarized microscope, fitted with a Canon G2 digital camera. For Congo red birefringence experiments, precipitates were incubated for 3 h in a 0.1 wt% Congo red solution. Afterwards, a drop of sample was covered with a microscope coverslip and observed through the crossed polarizers of the microscope.

2.8. X-ray diffraction (XRD)

Measurements were performed on stalks prepared by drying a drop of solution suspended between the ends of wax-coated capillaries. The stalks were mounted onto a four axis goniometer of an Oxford Diffraction Gemini Ultra instrument. The sample−detector distance was 50 mm and the X-ray wavelength was λ = 1.54 Å.

2.9. Cryogenic-TEM (Cryo-TEM)

Imaging was carried out using a field emission cryo-electron microscope (JEOL JEM-3200FSC), operating at 200 kV. Images were taken in bright field mode using zero loss energy filtering (omega type) with a slit width of 20 eV. Micrographs were recorded using a Gatan Ultrascan 4000 CCD camera. The specimen temperature was maintained at −187 °C during the imaging. Vitrified specimens were prepared using an automated FEI Vitrobot device using Quantifoil 3.5/1 holey carbon copper grids with a hole size of 3.5 μm. Just prior to use, grids were plasma cleaned using a Gatan Solarus 9500 plasma cleaner and then transferred into the environmental chamber of a FEI Vitrobot at room temperature and 100% humidity. Thereafter 3 μl of sample solution was applied on the grid and was blotted twice for 5 s and then vitrified in a 1/1 mixture of liquid ethane and propane at temperature of −180 °C. The grids with vitrified sample solution were maintained at liquid nitrogen temperature and then cryo-transferred to the microscope.

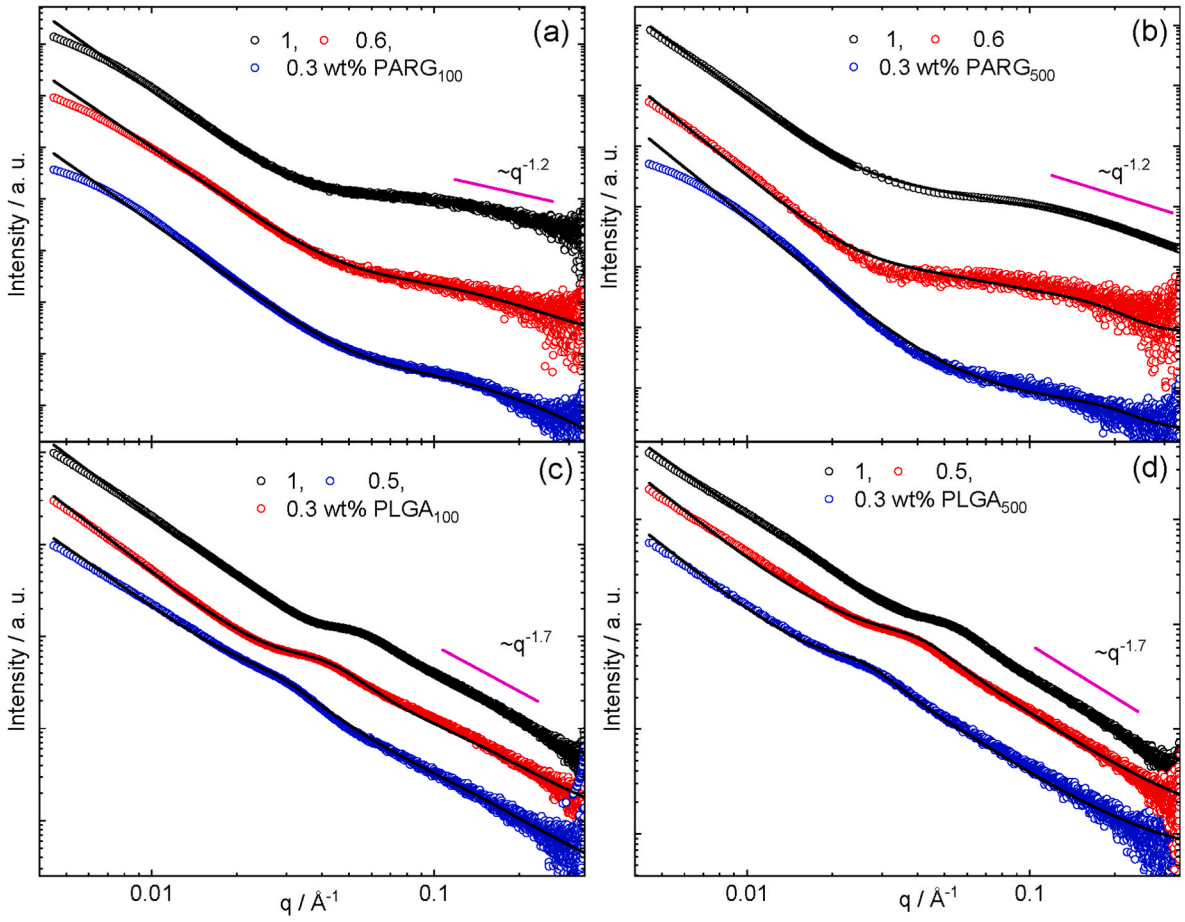

Fig. 1. SAXS data measured for (a) $PLGA_{100}$, (b) $PLGA_{500}$, (c) $PARG_{100}$ and (d) $PARG_{500}$ solutions in the range of concentrations (0.3–1) wt%. SAXS curves have been shifted in order to enable visualization.

2.10. Small angle X-ray scattering (SAXS)

Experiments were performed on beamline B21 (Diamond Light Source Ltd., UK) [25] and at beamline SWING (SOLEIL, France) [26]. On beamline B21, samples were loaded into the 96-well plate of an EMBL BioSAXS robot and then injected via an automated sample exchanger into a quartz capillary (1.8 mm internal diameter) in the X-ray beam. The quartz capillary was enclosed in a vacuum chamber. The flow of the sample through the capillary was continuous during the SAXS data acquisition. Beamline B21 operated with a fixed camera length (3.9 m) and a fixed wavelength ($\lambda = 1.00$ Å). The images were captured using a Pilatus 2 M detector. Data processing (background subtraction, radial averaging) was performed using the dedicated beamline software ScÅtter. On SWING, samples were delivered to a quartz capillary under vacuum in the x-ray beam using a BioSAXS setup. Data were collected using an in-vacuum EigerX-4M detector, with an x-ray wavelength 1.033 Å at two sample-to-detector distances, 6.217 m and 0.517 m. Data were reduced to one-dimensional form as a function of wavenumber $q = 4\pi\sin\theta/\lambda$ (where 2θ is the scattering angle) and averaged and background subtracted using the software Foxtrot [26].

2.11. SAXS models

The SAXS data was fitted using a form factor for a wormlike chain with excluded volume interactions [27]. In this model, a chain of contour length L is made of locally stiff segments of persistence length l_p. The Kuhn length $\xi = 2l_p$ describes the stiffness of the chain. The chain has a non-negligible circular cross section with radius R. The model allows for excluded volume interactions via R. In our fits we set $\xi = 8$ Å [16], equal to the measured value for PLGA ($\xi = 8$ Å) [28,29] and similar to that for modelled polypeptide chains ($\xi = 7.45$ Å in the inhomogeneous partially freely rotating chain model) [30]. We also set $L = 100$ or 500 for polymerization degree 100 or 500 respectively.

The radius of gyration of the cross section of polyelectrolytes in salt-free aqueous solution, $R_{g,c} = R/2^{1/2}$ has been previously measured by small angle scattering, and reported as $R_{g,c} = 3$ Å ($R = 4.2$ Å) for poly (styrene sulfonate) [31], and $R_{gc} = 5.1$ Å ($R = 7.2$ Å) for polyacrylic acid [32]. Here, we set $R = 5$ Å, corresponding to the average over the set of values obtained from the first round of fits to the SAXS curves. As previously reported in the literature for closely related systems [16], the low-q upturn in the SAXS intensity was described using the function $I(q) = C_0 + C_1 q^{-\alpha}$.

The structure factor was qualitatively described as a Lorentzian function, with amplitude A; position of peak maximum q_0; width W and background BG. In this model, $2\pi/q_0$ and $2\pi/W$ represent the average distance between interacting chains and correlation length respectively.

3. Results

We investigated the conformation and structure of polyelectrolyte complexes of poly(L-glutamic acid) (sodium salt) PLGA and poly(L-arginine) PARG (hydrobromide salt) (molecular structures shown in SI Scheme S1) for two pairs of molar masses, with average degrees of polymerization $n = 100$ and $n = 500$ respectively. The complexation was studied as a function of mixture stoichiometry and hence net charge. The net charges for the mixtures studied calculated using the Henderson-Hasselbalch equation assuming arginine pKa = 12.5 and glutamic acid pKa = 4 [24] are shown in SI Fig. S4. The pH was measured in the range

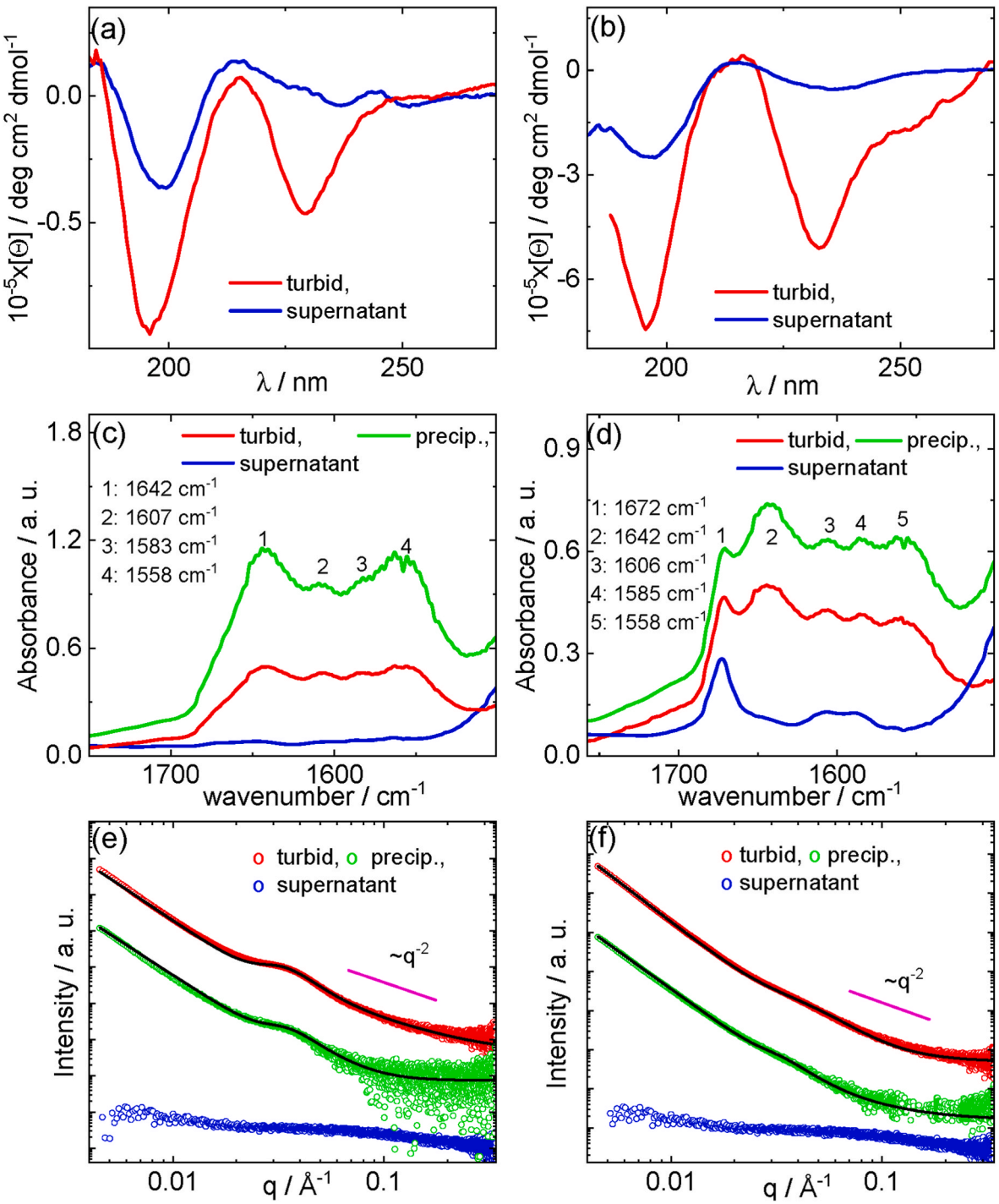

Fig. 2. Complexation at charge 0. CD data for re-suspended precipitate (turbid) and supernatant for samples (a) 1.3 wt% $PLGA_{100}$:1.1 wt% $PARG_{100}$ and (b) 1.3 wt% $PLGA_{500}$:1.1 wt% $PARG_{500}$. FTIR and SAXS data for resuspended precipitate, precipitate and supernatant for (c,e) 1.3 wt% $PLGA_{100}$:1.1 wt% $PARG_{100}$ and (d,f) 1.3 wt % $PLGA_{500}$:1.1 wt% $PARG_{500}$. SAXS curves have been shifted to enable visualization.

6–7 for the mixtures studied (SI Table S1) and according to the calculated net charge, this corresponds to net charge 0 for near equimolar mixtures and net charge −0.5 for the asymmetric mixtures 0.5 wt% PLGA:0.3 wt% PARG studied.

3.1. Homopolypeptides

Before presenting results for the polyelectrolyte complexes, we examined the conformation of the PLGA and PARG polymers studied using CD and SAXS. The results are compared to prior literature results. Circular dichroism spectra for all four polymers studied: $PLGA_{100}$, $PLGA_{500}$, $PARG_{100}$ and $PARG_{500}$ (the subscripts indicate the degree of polymerization, Table 1) are shown in Fig. S5. The spectra for both PLGA samples show features of polyproline II (PPII) conformation, i.e. a negative minimum at 197 nm and a positive maximum near 220 nm, as previously reported for PLGA at high pH [33,34]. The spectra for the two PARG samples show qualitatively similar features, although the negative minimum at 197 nm is less sharply defined. The maximum in the spectra in the range 210–220 nm has previously been observed for poly (L-arginine) in aqueous solution in a pH range 2.7–12 [35–38] and for

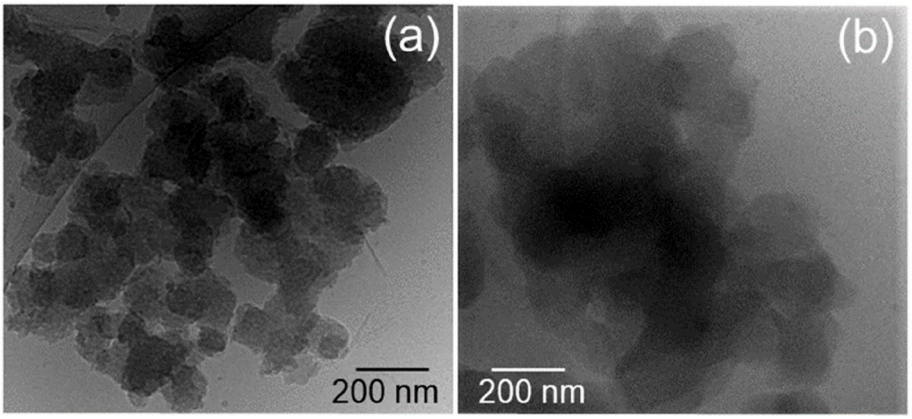

Fig. 3. Complexation at charge 0. Cryo-TEM images for (a) 1.3 wt% $PLGA_{100}$:1.1 wt% $PARG_{100}$ and (b) 1.3 wt% $PLGA_{500}$:1.1 wt% $PARG_{500}$.

aqueous salt solutions with pH 5.7–11.7 (where the minimum at 198 nm was also reported) [39]. Our CD results thus indicate that all four polyelectrolytes adopt PPII-like conformations in aqueous solution. FTIR was also used to examine the secondary structure of the polypeptides. The data is shown in SI Fig. S6. For the two PARG samples, the peaks at 1646-1647 cm^{-1} are consistent with polyproline II conformation (although it is difficult to distinguish PPII from disordered/random coil in FTIR spectra of peptides) [40,41]. The peaks at 1607-1610 cm^{-1} and 1587-1588 cm^{-1} are associated with polyarginine side chain (guanidyl group) modes [42–45]. The peak at 1672 cm^{-1} observed for $PARG_{500}$ is due to bound TFA counterions [46–48] and/or the presence of guanidyl groups in residual H_2O [42]. The peaks observed for both PLGA polymers at 1646-1647 cm^{-1} are similarly assigned to polyproline II while peaks at 1563-1564 cm^{-1} are due to COO stretch deformations in glutamic acid [42]. Thus FTIR is compatible with CD and indicates that the homopolyelectrolyte polypeptides have PPII structure.

We further used SAXS to measure the form and structure factors of the homopolyelectrolytes in aqueous solution to probe the conformation and packing of the extended polyelectrolytes. The SAXS data is shown in Fig. 1. As mentioned in the Experimental section, all data could be fitted using a model comprising the form factor of wormlike chains with a Lorentzian function to describe the structure factor peak observed for all samples except $PARG_{100}$. This model describes well the data for all four polymers, and the fit parameters are listed in SI Table S2 and SI Table S3. The structure factor peak arises from inter-chain correlations due to electrostatic repulsions in the polyelectrolyte solutions [20,49,50]. The peak shifts to higher q as concentration is increased [20]. This corresponds to a reduction in the domain spacing associated with the polyelectrolyte 'correlation hole' with concentration as shown in SI Fig. S7, which also shows empirical scaling relationships $d_0 \sim c^{-0.5}$. This is the behaviour observed for the polyelectrolyte peak for semidilute polyelectrolyte solutions ($c^{-1/2}$) [18,20].

The wormlike chain form factor resulting from the extended polypeptide conformation for PLGA shows an intensity scaling $I(q) \sim q^{-1/\nu} = q^{-1.7}$ at high q, which is due to the excluded volume behaviour (Flory exponent $\nu = 0.588$ predicted) [51] of the wormlike chains [27]. The high q scaling behaviour observed for the two PARG polymers is $I(q) \sim q^{-1.2}$, although this is likely to be influenced by the broad structure factor peak tails, since this peak is significantly broader (and at higher q) than the peak observed for the PLGA polymers, indicating a more disordered and shorter length scale correlated polyelectrolyte chain packing. In the fitting, the contour length was fixed at $L = 100$ Å for the two polymers $PARG_{100}$ and $PLGA_{100}$ and $L = 500$ Å for the $PARG_{500}$ and $PLGA_{500}$, for all three concentrations studied. These values are lower than those used in the wormlike chain form factor fitting of SAXS data from poly(L-lysine) with $n = 100$ and 400 and mixtures with poly(D, L-glutamic acid) [16]. The radius of the wormlike chains from the fits for solutions of all four polymers was fixed at $R = 5$ Å. This value is consistent with the effective radius of the backbone of the polyelectrolytes, as previously reported for PLGA sodium salt [29,52] as well as poly(D-glutamic acid) in aqueous solutions [53]. To the best of our knowledge, SAXS data has not previously been described for poly (L-arginine), although reported SAXS measurements for oligo(arginine) show a polyelectrolyte structure factor peak (the form factor was not analysed) [54].

3.2. Mixtures of polypeptides

Having established using CD spectroscopy that all four polymers adopt PPII-like structures and have extended conformations describable using a wormlike chain conformation in modelling SAXS form factors (with additional polyelectrolyte structure factor peaks), we now turn to examine the behaviour of mixtures of pairs of PLGA/PARG polymers (with matched molar masses) as a function of stoichiometry which in turn controls the net charge on polyelectrolyte complexes formed. We first consider the case of a near equimolar mixture (expected net charge 0). These were found to form solid complexes and precipitates were observed (SI Fig. S8). The data from CD, FTIR and SAXS are shown in Fig. 2 for the precipitate, resuspended precipitate and supernatant for comparison. The CD spectra for both pairs of polymers ($n = 100$ and $n = 500$) are qualitatively similar. The spectra have features of PPII (negative minimum at 197 nm and positive maximum near 220 nm), as discussed above for the homopolyelectrolytes. This is more enhanced in the spectra for the mixtures compared to the homopolymers, especially for the resuspended precipitate. This may be due to a contribution from β-sheet structure which leads to a minimum in the CD spectrum, expected at 216 nm [55–57] but red-shifted due to aggregation, leading to a minimum near 230 nm in the spectra in Fig. 2a and b. FTIR spectra shown in Fig. 2c and d for the precipitate or resuspended precipitate contain peaks similar to those for the homopolypeptides discussed above, i.e. there is a peak due to PPII at 1642 cm^{-1} and the other peaks are specific to the glutamic acid and arginine side chain vibrational modes. The spectra for the supernatants show weaker and broader peaks. The SAXS data shown in Fig. 2e and f shows form factor features for the supernatant that can be ascribed to unaggregated monomers, however for the precipitate (or resuspended precipitate) there are additional polyelectrolyte structure factor peaks on top of a power-law like form factor profile with terminal $I(q) \sim q^{-2}$ behaviour. This data was fitted to a power-law form factor and the fit parameters are listed in SI Table S4. The power-law form is consistent with fractal-like structures which were observed in cryo-TEM images for both n = 100 and n = 500 equimolar mixtures shown in Fig. 3. For the resuspended precipitates, globular aggregates of 100–200 nm diameter can be seen which have an internal multi-compartment fractal-like structure. The data in Figs. 2 and 3 thus suggest that the precipitates in solution have predominantly a globular fractal-like structure based on PPII polypeptide conformation.

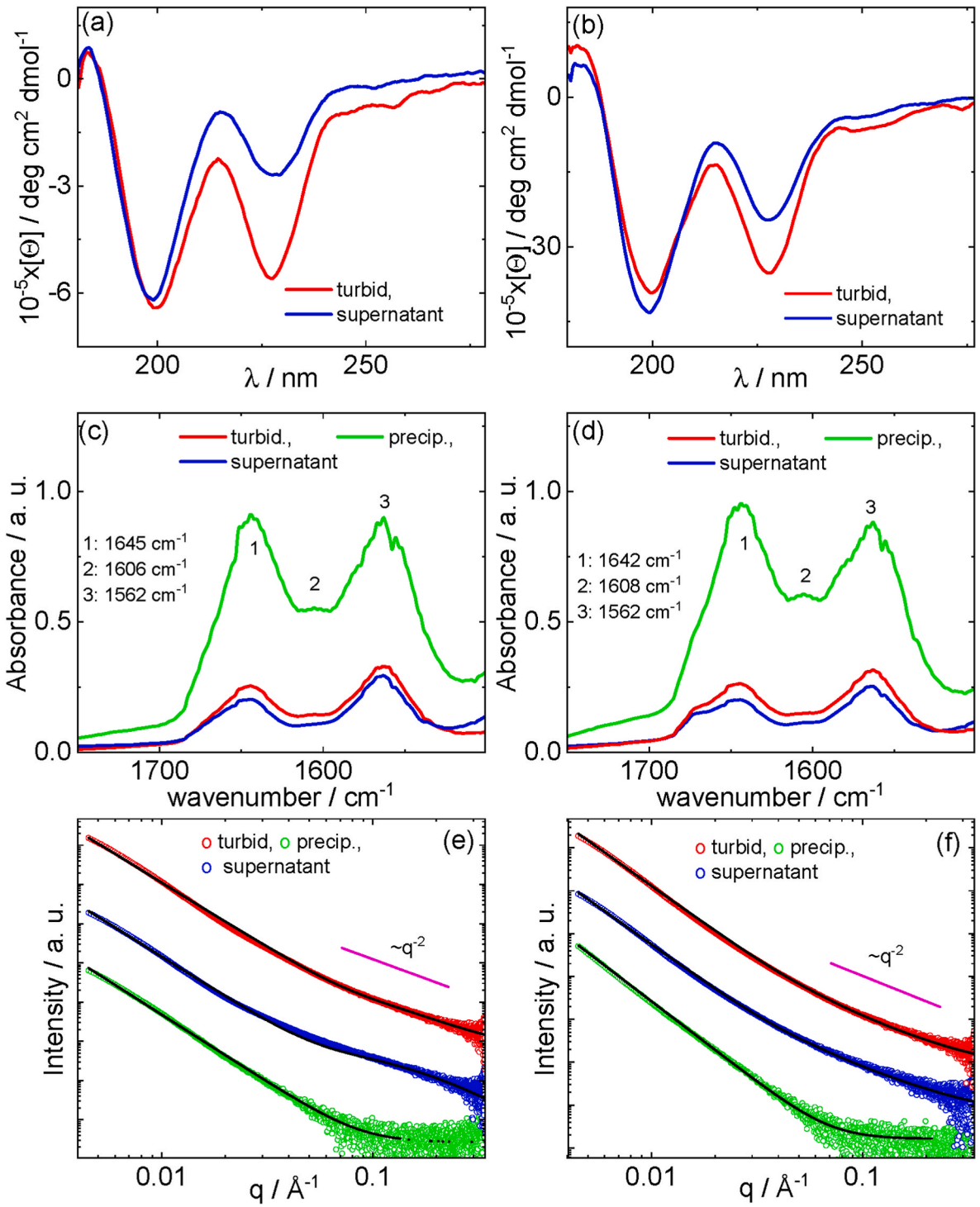

Fig. 4. Complexation at charge −0.5. CD data for re-suspended precipitate (turbid) and supernatant for samples (a) 0.5 wt% $PLGA_{100}$:0.3 wt% $PARG_{100}$ and (b) 0.5 wt% $PLGA_{500}$:0.3 wt% $PARG_{500}$. FTIR and SAXS data for resuspended precipitate, precipitate and supernatant for (c,e) 0.5 wt% $PLGA_{100}$:0.3 wt% $PARG_{100}$ and (d,f) 0.5 wt% $PLGA_{500}$:0.3 wt% $PARG_{500}$. SAXS curves have been shifted to enable visualization.

There is little evidence for β-sheet structure.

However, a careful examination of dried precipitates and *in situ* extended *q*-range SAXS on suspended precipitates did reveal evidence for a component of β-sheet structure, which seems to be enhanced upon drying the precipitates. SI Fig. S9 contains data from XRD on dried stalks, and SI Fig. S10 shows polarized optical microscopy images of partly dried precipitates. The XRD data contains peaks at 4.9 Å due to the β-strand spacing in a β-sheet structure, this is much more pronounced for the $n = 100$ system. The other peaks can be indexed according to the published powder XRD structures for β-sheet PARG [58] and PLGA [59]. The POM images show birefringent nematic-like structures (and spherulites), which must arise from the presence of some aligned superstructure such as β-sheet fibrils. This is further confirmed by staining with the amyloid-sensitive dye Congo red [57,60] which gives green birefringence in POM (SI Fig. S10a). As a powerful *in situ* nanostructural probe, extended *q*-range SAXS was performed on resuspended precipitates. The data is shown in SI Fig. S11 and SI Fig. S12 for the net charge 0 and net charge −0.5 mixtures. The data extend to

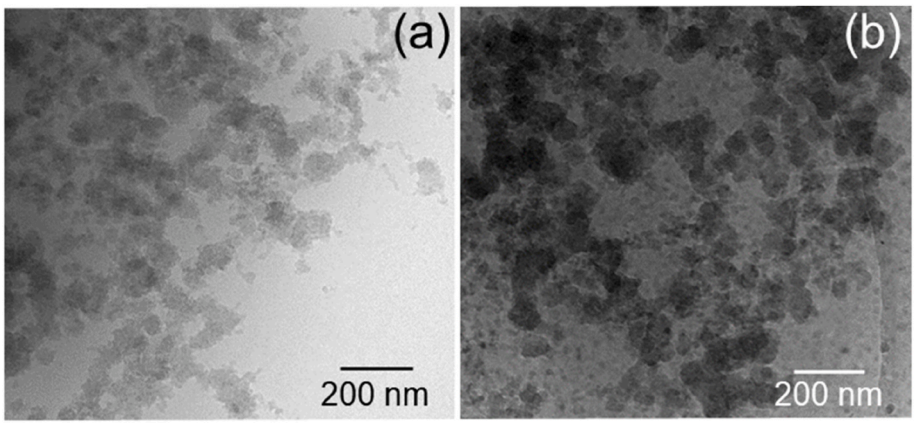

Fig. 5. Complexation at charge −0.5. Cryo-TEM images for (a) 0.5 wt% $PLGA_{100}$:0.3 wt% $PARG_{100}$ and (b) 0.5 wt% $PLGA_{500}$:0.3 wt% $PARG_{500}$.

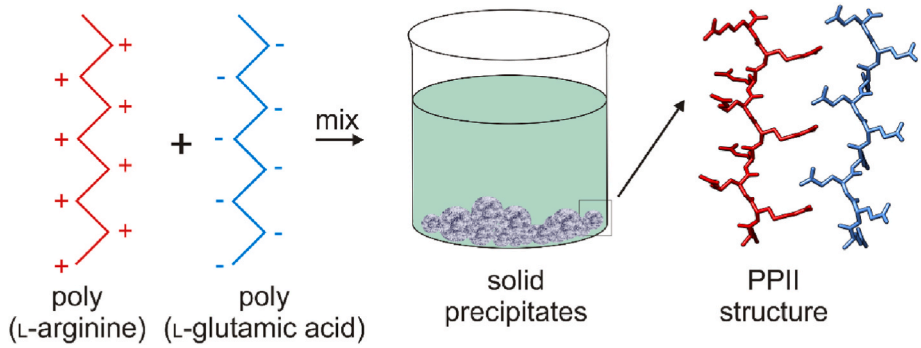

Fig. 6. Schematic of precipitate formation in the mixtures of PARG and PLGA studied, showing PPII conformations of the polymer chains.

high q and enable the resolution of peaks due to secondary structure in the aqueous suspensions of precipitates. The data shows features due to 'cross-β' structure [57,61], i.e. inter-strand spacings of 4.7–4.9 Å due to the inter-strand spacing, and 9.7–16.4 Å associated with the β-sheet spacing and width. The peak at 6.5–6.7 Å is assigned to the PARG β-structure unit cell c-axis length [58]. The peaks observed in the *in situ* SAXS profile are also consistent with those in the XRD profiles (SI Fig. S9). Thus, we can conclude based on evidence from powder XRD, POM, Congo red staining and *in situ* SAXS that there is a component of β-sheet structure in the resuspended fibrils. However, CD and FTIR spectroscopy (Fig. 2a–d) indicate that this is not the major conformation of the polypeptide chains in the complexes in solution.

Fig. 4 shows CD, FTIR and SAXS data for a net charge −0.5 mixture (samples shown in Figs. S8c and d). The spectra show features similar to those discussed for the net charge 0 system (data in Fig. 2), i.e. the CD spectra for both supernatant and suspended precipitate contain a predominant contribution from PPII structure. The FTIR spectra contain peaks at 1642-1645 cm^{-1} due to PPII secondary structure with peaks at 1606-1608 cm^{-1} due to arginine side chain modes and at 1562 cm^{-1} due to glutamic acid carboxylate vibrations, as indexed above for the homopolypeptides. The SAXS data in Fig. 4e and f was fitted using the same fractal-like structure used for the data in Fig. 2e and f. There is a terminal q^{-2} slope, however a distinctive feature is the lack of a polyelectrolyte structure factor peak, and the presence of a contribution to the form factor from wormlike chains. The fit parameters are listed in SI Table S5. Consistent with the lower degree of precipitation observed for the net charge −0.5 samples, cryo-TEM (Fig. 5) reveals smaller and more diffuse aggregates than those in Fig. 3 for the net charge 0 complexes.

Our results suggest that precipitate formation is driven by PARG which is more hydrophobic as compared to PLGA. This is because samples with higher content of PARG show more extensive precipitate formation. The precipitates contain peptide that is predominantly in a PPII conformation as shown in the Schematic in Fig. 6.

4. Conclusions

In summary, our studies show that low molar mass PLGA and PARG homopolypeptides adopt a PPII-like conformation of extended polyelectrolyte chains. This conformation is largely retained in complexes of the two peptides which form precipitates in the net charge 0 and net charge −0.5 mixtures studied. There is a greater degree of precipitation at net charge zero and there is evidence for some β-sheet structure in dried samples of the precipitates formed. The predominant structure in the precipitates however is PPII with globular aggregates with internal 'blob' structure visualized using cryo-TEM and giving a fractal-like form factor component. The polyelectrolyte structure factor is retained. Tirrell's group previously presented FTIR data as evidence for β-sheet structure in precipitates of poly(L-lysine) and poly(glutamic acid) (of matching or opposite chirality) [15]. Here, we complement FTIR and CD data with XRD, *in situ* SAXS and POM, since the FTIR data is inconclusive for our system due to the coincidence of an arginine side chain mode near 1608 cm^{-1} with peaks at 1611-1613 cm^{-1} assigned to β-sheet modes, which in poly(L-lysine)/poly(L-glutamic acid) complexes were also accompanied by a shoulder feature near 1680 cm^{-1} due to antiparallel β-sheet structure [15].

It is important to note that our studies on the conformation of PLGA and PARG are for well-defined custom synthesized low molar mass polymers, extending to the very low molar mass limit for the $n = 100$ samples. This is in contrast to much prior work which has used commercial samples, in particular PLGA polymers with molar masses $>1 \times 10^4$ g mol^{-1} from Sigma-Aldrich [29,52] or polymers synthesized with masses also above this limit [53,59]. In addition, several studies used Sigma-Aldrich poly(L-arginine) hydrochloride (PARG) with $M_w = 40$ kg mol^{-1} or more [36,37,39] or NCA-polymerized samples with $M > 10^4$ g

mol^{-1} [58]. However, the PARG studied by CD by Hayakawa et al. has estimated $n = 70$ [35] and Tirrell's group studied PLGA and P(L-lysine) (and other enantiomers) with $n = 100$ and $n = 400$ [7,16].

Polyelectrolyte complexes are the focus of intense research due to the known involvement of coacervates in cellular processes and origin of life scenarios. Solid polyelectrolyte complexes are less studied but may also be relevant to the understanding of intra or inter-cellular bodies such as those formed by amyloid proteins and peptides (Lewy and other inclusion bodies) [62].

As well as being a model cationic polyelectrolyte, polyarginine is of future interest since oligo- and poly-arginines have cell-penetrating properties and can be used to deliver DNA into cells and have additional activity as antimicrobial materials, for wound healing and in the fabrication of layer-by-layer microcapsules for drug delivery [8,39,45,63,64].

CRediT authorship contribution statement

Valeria Castelletto: Methodology, Investigation, Formal analysis, Writing – original draft, preparation, Writing – review & editing, Visualization. **Lucas de Mello:** Investigation. **Foteini Arfara:** Investigation, Visualization. **Hermis Iatrou:** Investigation, Resources, Visualization, Writing – original draft, preparation, Supervision. **Jani Seitsonen:** Investigation, Visualization. **Ian W. Hamley:** Conceptualization, Investigation, Resources, Formal analysis, Visualization, Writing – original draft, preparation, Writing – review & editing, Supervision, Project administration, Funding acquisition.

Declaration of competing interest

The authors declare that they have no known competing financial interests or personal relationships that could have appeared to influence the work reported in this paper.

Data availability

Data will be made available on request.

Acknowledgements

This work was supported by EPSRC Fellowship grant EP/V053396/1 to IWH, and by the European Union and Greek national funds through the Operational Program "Competitiveness, Entrepreneurship and Innovation", under the call "RESEARCH-CREATE-INNOVATE" (project code: T1EΔK-01833). We are grateful for the award of synchrotron SAXS beamtime at SOLEIL (proposal no. 20211309) and the support of Thomas Bizien (SOLEIL) and Elisabetta Rosa (University of Naples *Federico II*, Italy) during the measurements. Beamtime at Diamond was awarded under reference SM29895-1 and we thank Nikul Khunti for assistance. We acknowledge access to instruments of the Chemical Analysis Facility at the University of Reading.

Appendix A. Supplementary data

Supplementary data to this article can be found online at https://doi.org/10.1016/j.polymer.2022.125497.

References

[1] A.I. Oparin, The Origin of Life, Dover, 1953.
[2] S. Koga, D.S. Williams, A.W. Perriman, S. Mann, Peptide-nucleotide microdroplets as a step towards a membrane-free protocell model, Nat. Chem. 3 (2011) 720–724.
[3] A.J. Dzieciol, S. Mann, Designs for life: protocell models in the laboratory, Chem. Soc. Rev. 41 (2012) 79–85.
[4] D.S. Williams, S. Koga, C.R.C. Hak, A. Majrekar, A.J. Patil, A.W. Perriman, S. Mann, Polymer/nucleotide droplets as bio-inspired functional micro-compartments, Soft Matter 8 (2012) 6004–6014.
[5] A.A. Hyman, C.A. Weber, F. Juelicher, LIquid-liquid phase separation in biology, in: R. Schekman, R. Lehmann (Eds.) Annual Review of Cell and Developmental Biology, Vol vol. 302014, pp. 39-58.
[6] Y. Shin, C.P. Brangwynne, Liquid phase condensation in cell physiology and disease, Science 357 (2017).
[7] L. Li, S. Srivastava, M. Andreev, A.B. Marciel, J.J. de Pablo, M.V. Tirrell, Phase behavior and salt partitioning in polyelectrolyte complex coacervates, Macromolecules 51 (2018) 2988–2995.
[8] K. Ariga, Y.M. Lvov, K. Kawakami, Q.M. Ji, J.P. Hill, Layer-by-layer self-assembled shells for drug delivery, Adv. Drug Deliv. Rev. 63 (2011) 762–771.
[9] Q. Zhao, Q.F.F. An, Y.L. Ji, J.W. Qian, C.J. Gao, Polyelectrolyte complex membranes for pervaporation, nanofiltration and fuel cell applications, J. Membr. Sci. 379 (2011) 19–45.
[10] A.M. Rumyantsev, N.E. Jackson, J.J. de Pablo, Polyelectrolyte complex coacervates: recent developments and new frontiers, in: A.P. Mackenzie, M. C. Marchetti (Eds.), Annual Review of Condensed Matter Physics 12 (2021) (2021) 155–176.
[11] P.M. Biesheuvel, M.A.C. Stuart, Electrostatic free energy of weakly charged macromolecules in solution and intermacromolecular complexes consisting of oppositely charged polymers, Langmuir 20 (2004) 2785–2791.
[12] R. Chollakup, W. Smitthipong, C.D. Eisenbach, M. Tirrell, Phase behavior and coacervation of aqueous poly(acrylic acid)-Poly(allylamine) solutions, Macromolecules 43 (2010) 2518–2528.
[13] S. Adhikari, M.A. Leaf, M. Muthukumar, Polyelectrolyte complex coacervation by electrostatic dipolar interactions, J. Chem. Phys. 149 (2018).
[14] A.E. Neitzel, G.X. de Hoe, M.V. Tirrell, Expanding the structural diversity of polyelectrolyte complexes and polyzwitterions, Curr. Opin. Solid State Mater. Sci. 25 (2021).
[15] S.L. Perry, L. Leon, K.Q. Hoffmann, M.J. Kade, D. Priftis, K.A. Black, D. Wong, R. A. Klein, C.F. Pierce, K.O. Margossian, J.K. Whitmer, J. Qin, J.J. de Pablo, M. Tirrell, Chirality-selected phase behaviour in ionic polypeptide complexes, Nat. Commun. 6 (2015).
[16] A.B. Marciel, S. Srivastava, M.V. Tirrell, Structure and rheology of polyelectrolyte complex coacervates, Soft Matter 14 (2018) 2454–2464.
[17] J.C. Fu, J.B. Schlenoff, Driving forces for oppositely charged polyion association in aqueous solutions: enthalpic, entropic, but not electrostatic, J. Am. Chem. Soc. 138 (2016) 980–990.
[18] M. Muthukumar, 50th anniversary perspective: a perspective on polyelectrolyte solutions, Macromolecules 50 (2017) 9528–9560.
[19] H. Dautzenberg, Polyelectrolyte complex formation in highly aggregating systems. 1. Effect of salt: polyelectrolyte complex formation in the presence of NaCl, Macromolecules 30 (1997) 7810–7815.
[20] J. Combet, P. Lorchat, M. Rawiso, Salt-free aqueous solutions of polyelectrolytes: small angle X-ray and neutron scattering characterization, Eur. Phys. J. Spec. Top. 213 (2012) 243–265.
[21] Q.F. Wang, J.B. Schlenoff, The polyelectrolyte complex/coacervate continuum, Macromolecules 47 (2014) 3108–3116.
[22] T.M. Lu, E. Spruijt, Multiphase complex coacervate droplets, J. Am. Chem. Soc. 142 (2020) 2905–2914.
[23] J. Zhu, L. Jiang, Liquid-liquid phase separation bridges physics, chemistry, and biology, Langmuir 38 (2022) 9043–9049.
[24] I.W. Hamley, Introduction to Peptide Science, Wiley, Chichester, 2020.
[25] N.P. Cowieson, C.J.C. Edwards-Gayle, K. Inoue, N.S. Khunti, J. Doutch, E. Williams, S. Daniels, G. Preece, N.A. Krumpa, J.P. Sutter, M.D. Tully, N.J. Terrill, R.P. Rambo, Beamline B21: high-throughput small-angle X-ray scattering at Diamond light Source, J. Synchrotron Radiat. 27 (2020) 1438–1446.
[26] A. Thureau, P. Roblin, J. Perez, BioSAXS on the SWING beamline at synchrotron SOLEIL, J. Appl. Crystallogr. 54 (2021) 1698–1710.
[27] J.S. Pedersen, P. Schurtenberger, Scattering functions of semi-flexible polymers with and without excluded volume effects, Macromolecules 29 (1996) 7602–7612.
[28] R.B. Hawkins, A. Holtzer, Some macromolecular properties of poly(a-L-glutamic acid) random coils, Macromolecules 5 (1972) 294–301.
[29] S. Shimizu, Y. Muroga, S. Iida, M. Miyahara, M. Ishibashi, H. Ikake, K. Kurita, SAXS studies on added-salt species dependence of conformation of fully-charged poly(L-glutamate) in aqueous solutions, in: 14th International Conference on Small-Angle Scattering, SAS09), Oxford, ENGLAND, 2009.
[30] F. Hanke, A. Serr, H.J. Kreuzer, R.R. Netz, Stretching single polypeptides: the effect of rotational constraints in the backbone, EPL (2010) 92.
[31] J. Combet, Polyelectrolytes and small angle scattering, EPJ Web Conf. 188 (2018), 03001.
[32] T.J. Taylor, S.S. Stivala, Small-angle X-ray scattering study of a weak polyelectrolyte in water, J. Polym. Sci. B Polym. Phys. 41 (2003) 1263–1272.
[33] M.L. Tiffany, S. Krimm, New Chain Conform. Poly(glutamic Acid) and Polylysine Biopolym. 6 (1968) 1379–1382.
[34] S. Krimm, J.E. Mark, Conformations of polypeptides with ionized side chains of equal length, Proc. Nat. Acad. Sci USA 60 (1968) 1122–1129.
[35] T. Hayakawa, Y. Kondo, H. Yamamoto, Secondary structure of poly-L-arginine and its derivatives, Bull. Chem. Soc. Jpn. 42 (1969) 1937–1941.
[36] A.J. Stipanovic, E.S. Stevens, Vacuum ultraviolet circular-dichroism of chondroitins and their complexes with poly(L-arginine), Biopolymers 20 (1981) 1565–1573.
[37] Y. Takechi, H. Yoshii, M. Tanaka, T. Kawakami, S. Aimoto, H. Saito, Physicochemical mechanism for the enhanced ability of lipid membrane penetration of polyarginine, Langmuir 27 (2011) 7099–7107.
[38] S. General, A.F. Thunemann, pH-sensitive nanoparticles of poly(amino acid) dodecanoate complexes, Int. J. Pharmaceutics 230 (2001) 11–24.

[39] M. Morga, P. Batys, D. Kosior, P. Bonarek, Z. Adamczyk, Poly-L-arginine molecule properties in simple electrolytes: molecular dynamic modeling and experiments, Int. J. Environ. Res. Publ. Health 19 (2022).
[40] T.A. Keiderling, Q. Xu, Unfolded Peptides and Proteins Studied with Infrared Absorption and Vibrational Circular Dichroism Spectra, Academic Press, San Diego, 2002.
[41] V. Castelletto, I.W. Hamley, C. Cenker, U. Olsson, J. Adamcik, R. Mezzenga, J. F. Miravet, B. Escuder, F. Rodriguez-Llansola, Influence of end-capping on the self-assembly of model amyloid peptide fragments, J. Phys. Chem. B 115 (2011) 2107–2116.
[42] A. Barth, The infrared absorption of amino acid side chains, Prog. Biophys. Mol. Biol. 74 (2000) 141–173.
[43] A. Barth, C. Zscherp, What vibrations tell us about proteins, Quater. Rev. Biophys. 35 (2002) 369–430.
[44] A. Ghosh, M.J. Tucker, R.M. Hochstrasser, Identification of arginine residues in peptides by 2D-IR echo spectroscopy, J. Phys. Chem. A 115 (2011) 9731–9738.
[45] C.J.C. Edwards-Gayle, V. Castelletto, I.W. Hamley, G. Barrett, F. Greco, D. Hermida-Merino, R. Rambo, J. Seitsonen, J. Ruokolainen, Self-assembly, antimicrobial activity and membrane interactions of arginine-capped peptide bola-amphiphiles, ACS Appl. Bio Mater. 2 (2019) 2208–2218.
[46] J.T. Pelton, L.R. McLean, Spectroscopic methods for analysis of protein secondary structure, Anal. Biochem. 277 (2000) 167–176.
[47] H. Gaussier, H. Morency, M.C. Lavoie, M. Subirade, Replacement of trifluoroacetic acid with HCl in the hydrophobic purification steps of pediocin PA-1: a structural effect, Appl. Environ. Microbiol. 68 (2002) 4803–4808.
[48] F. Eker, K. Griebenow, R. Schweitzer-Stenner, Ab_{1-28} fragment of the amyloid peptide predominantly adopts a polypropyline II conformation in acidic solution, Biochem 43 (2004) 6893–6898.
[49] J.P. Cotton, M. Moan, Inter-polyionic orientation in polyelectrolyte solution, observed by small-angle neutron-scattering, J. Phys., Lett. 37 (1976) L75–L77.
[50] M. Nierlich, C.E. Williams, F. Boue, J.P. Cotton, M. Daoud, B. Farnoux, G. Jannink, C. Picot, M. Moan, C. Wolff, M. Rinaudo, P.G.D. Gennes, Small-angle neutron-scattering by semi-dilute solutions of polyelectrolyte, J. Phys. France 40 (1979) 701–704.
[51] P.G. de Gennes, Scaling Concepts in Polymer Physics, Cornell University Press, Ithaca, 1979.
[52] S. Shimizu, Y. Muroga, T. Hyono, K. Kurita, Small-angle X-ray scattering study on conformation of poly(sodium L-glutamate) in NaCl and NaF aqueous solutions, J. Appl. Crystallogr. 40 (2007) S553–S557.
[53] Y. Muroga, H. Tagawa, Y. Hiragi, T. Ueki, M. Kataoka, Y. Izumi, Y. Amemiya, Conformational analysis of broken rodlike chains .2. Conformational-analysis of poly(D-glutamic acid) in aqueous-solution by small-angle X-ray-scattering, Macromolecules 21 (1988) 2756–2760.
[54] G. Tesei, M. Vazdar, M.R. Jensen, C. Cragnell, P.E. Mason, J. Heyda, M. Skepo, P. Jungwirth, M. Lund, Self-association of a highly charged arginine-rich cell-penetrating peptide, Proc. Nat. Acad. Sci USA 114 (2017) 11428–11433.
[55] R.W. Woody, Circular dichroism of peptides and proteins, in: K. Nakanishi, N. Berova, R.W. Woody (Eds.), Circular Dichroism. Principles and Applications, VCH, New York, 1994, pp. 473–496.
[56] A. Rodger, B. Nordén, Circular Dichroism and Linear Dichroism, Oxford University Press, Oxford, 1997.
[57] I.W. Hamley, Peptide fibrillisation, Angew. Chem. 46 (2007) 8128–8147.
[58] M. Suwalsky, W. Traub, An X-ray diffraction study of poly-L-arginine hydrochloride, Biopolymers 11 (1972) 623–&.
[59] H. Pivcova, V. Saudek, P. Schmidt, D. Hlavata, J. Plestil, F. Laupretre, Conformation of poly(glutamic acid) and of poly(aspartic acid) in the solid-state - X-ray-diffraction, infrared and ^{13}C cross-polarization magic angle spinning nuclear-magnetic-resonance spectroscopic study, Polymer 28 (1987) 991–997.
[60] A.K. Buell, C.M. Dobson, T.P.J. Knowles, M.E. Welland, Interactions between amyloidophilic dyes and their relevance to studies of amyloid inhibitors, Biophys. J. 99 (2010) 3492–3497.
[61] O.S. Makin, L.C. Serpell, Structures for amyloid fibrils, FEBS J. 272 (2005) 5950–5961.
[62] I.W. Hamley, The amyloid beta peptide: a chemist's perspective. Role in alzheimer's and fibrillization, Chem. Rev. 112 (2012) 5147–5192.
[63] D.I. Chan, E.J. Prenner, H.J. Vogel, Tryptophan- and arginine-rich antimicrobial peptides: structures and mechanisms of action, Biochim. Biophys. Acta, Biomembr. 1758 (2006) 1184–1202.
[64] C.J.C. Edwards-Gayle, G. Barrett, S. Roy, V. Castelletto, J. Seitsonen, J. Ruokolainen, I.W. Hamley, Selective antibacterial activity and lipid membrane interactions of arginine-rich amphiphilic peptides, ACS Appl. Bio Mater. 3 (2020) 1165–1175.